Tunable Negative Permeability in a Three-Dimensional Superconducting Metamaterial

C. Kurter,[1,2] T. Lan,[1,3] L. Sarytchev,[1] and Steven M. Anlage[1,4]
[1]Center for Nanophysics and Advanced Materials, Department of Physics, University of Maryland, College Park, Maryland 20742-4111, USA
[2]Department of Physics, Missouri University of Science and Technology, Rolla, Missouri 65409, USA
[3]Department of Materials Science and Engineering, Northwestern University, Evanston, Illinois 60208, USA
[4]Department of Electrical and Computer Engineering, University of Maryland, College Park, Maryland 20742-3285, USA
(Received 24 December 2014; revised manuscript received 27 March 2015; published 28 May 2015)

We report on highly tunable radio-frequency (rf) characteristics of a low-loss and compact three-dimensional (3D) metamaterial made of superconducting thin-film spiral resonators. The rf transmission spectrum of a single element of the metamaterial shows a fundamental resonance peak at ~24.95 MHz that shifts to a 25% smaller frequency and becomes degenerate when a 3D array of such elements is created. The metamaterial shows an *in situ* tunable narrow frequency band in which the real part of the effective permeability is negative over a wide range of temperature. This narrow frequency band gradually possesses near-zero and positive values for the real part of permeability as the superconducting critical temperature is approached. The studied 3D metamaterial can be used for increasing power-transfer efficiency and tunability of electrically small rf antennas.

DOI: 10.1103/PhysRevApplied.3.054010

I. INTRODUCTION

A three-dimensional (3D) array of subwavelength elements composing a metamaterial can demonstrate unique electromagnetic properties which are not directly accessible in nature, such as negative permeability [1,2] and zero refractive index [3,4]. Most metamaterials achieve these unusual effects by means of tailored geometrical structures without relying on the intrinsic properties of materials used in metamaterial fabrication. Conducting nonmagnetic split-ring resonators (SRRs), and their derivatives, are employed to demonstrate negative permeability by strongly coupling to the magnetic-field component of incident electromagnetic waves at microwave [5] or higher frequency bands [6,7]. However, when lower operational frequencies are needed, these resonator-based metamaterials require impractically large dimensions to be able to compensate for ohmic losses [8]. One way to address this miniaturization problem is to use superconductors since they show very low surface resistance below their transition temperatures [9,10]. Moreover, tunability of the resonant features can be precisely achieved without lumped elements by means of temperature and magnetic field [11–13]. For instance, the plasma frequency of superconducting spiral meta-atoms is tuned to the MHz range by means of temperature variation, and the plasmonic properties are studied at essentially fixed frequency [14].

Of particular interest are radio frequency (rf) metamaterials, where the free-space wavelength λ_0 can be tens of meters. Despite the challenge of scaling the dimensions down, rf metamaterials offer a wide spectrum of applications including high-resolution magnetic resonance imaging [15–17], magnetoinductive lenses [18], and wireless communication [19–22] employing electrically small antennas. Antennas integrated with compact rf metamaterials were speculated to have enhanced radiation power, high directivity, and reduced return loss due to the unique electromagnetic properties of metamaterials [23,24]. Ziolkowski [25,26] has proposed using a metamaterial with negative refractive index to boost the real radiated power of an electrically short dipole antenna (size, $\lambda_0/1000$) by almost 2 orders of magnitude compared to the dipole-in-free-space case. A large imaginary part (reactance) of radiation impedance $Z_{\mathrm{rad}} = R_{\mathrm{rad}} + iX_{\mathrm{rad}}$ of an electrically small antenna limits the radiation efficiency because free space has a purely real impedance [27]. When the antenna is placed in near-field proximity to a negative refractive index medium, the X_{rad} of the antenna can be canceled out. Therefore, the metamaterial acts as a natural impedance-matching network for the dipole, which maximizes the transfer of power from the antenna to free space in the far field. The bandwidth and the operating frequency of the antennas can also be reconfigured with tunable metamaterials, which is crucial for modern wireless communication systems relying on multiband operation [24].

In this work, we demonstrate a tunable 3D rf metamaterial composed of electrically small ($\sim\lambda_0/2300$) superconducting thin-film resonators. The single resonant element is a planar spiral constructed by $w = 3$ μm wide semicircular strips with increasing radii. The center-to-center separation between two adjacent turns is $s = 6$ μm.

The spiral is densely packed with a large number of turns, $N = 200$, where the inner and outer diameters are $D_i = 4.606$ mm and $D_o = 7$ mm, respectively. The electromagnetic response of the resonant spirals can be studied with a simple circuit model [28]; i.e., an individual planar spiral can be treated as a magnetic resonator with an angular resonant frequency of $\omega_0 = 1/\sqrt{LC}$, where L and C are the total inductance and capacitance, respectively.

Possessing large geometrical inductance and capacitance (due to a large number of turns) over a compact geometry puts the individual spirals into a significantly subwavelength self-resonance regime. Therefore, the metamaterial formed by the 3D array of these spirals can be considered as a continuous effective medium characterized with effective constitutive parameters; i.e., frequency-dependent permeability $\mu_{\text{eff}}(\omega)$ and permittivity $\epsilon_{\text{eff}}(\omega)$. Previous theoretical [29] and experimental [30,31] work on metamaterials with periodic circular conducting elements shows that the fundamental resonant frequency of the metamaterial can be drastically lower than that of the single constitutive element, mainly due to the mutual inductance (magnetic coupling) between the resonant elements. However, electrical (capacitive) coupling can also play a role in the collective electromagnetic response of the metamaterial; thus, interaction between the individual elements can be complex, depending on structural details of the metamaterial, such as separation between the resonant elements along the substrate, interlayer spacing, array size, and alignment or arrangement of the elements along the stacking direction [32,33].

Here we study a 3D superconducting metamaterial with subwavelength spiral elements operating in the rf regime. We find that the mutual interactions between the individual spirals contributes to the effective response of the macroscopic 3D metamaterial. Moreover, we observe that both the center frequency of the resonant bandwidth in the rf transmission and the negative $\mu_{\text{eff}}(\omega)$ region are highly temperature tunable.

II. EXPERIMENT

The metamaterial is patterned out of a 200-nm-thick Nb thin film sputtered onto a 350-μm-thick quartz substrate. We define circular spiral-shaped resonators [8] into the Nb film by using standard photolithography and reactive ion etching using a mixture of CF_4 and O_2 (10% O_2). After fabrication, the quartz substrates are diced into 0.9×0.9 cm^2 and 2.6×5.2 cm^2 pieces to have individual spirals and 2D arrays of 3×6 Nb spirals. To be able to extend the structure into three dimensions, four substrates containing 2D arrays are stacked along the c axis of the substrate by using thin sheets of Rohacell foam as spacers. The planes of the spirals are aligned in parallel and each substrate is separated from the next by 0.5 mm along the z direction to produce strong coupling between the Nb spirals in the third dimension. The experiments are conducted in an evacuated probe inside a cryogenic Dewar and the temperature is precisely adjusted by a temperature controller between 4.2 K up to well above the superconducting transition temperature, $T_c \simeq 9.2$ K of Nb.

III. RESULTS AND DISCUSSION

Figure 1 shows the rf transmission $|S_{12}|$ through a single Nb spiral along with the 2D and 3D arrays of the coupled spirals. The measurements are performed by means of two loop antennas sandwiching the samples (see the sketch in the inset of Fig. 1, illustrating the 3D array of spirals between the antennas; the quartz substrates are not shown). The antennas are made of semirigid coaxial cables by shaping the inner conductors into 1.2-cm-diameter loops and attaching them to the outer conductors. The other ends of the coaxial cables are connected to a two-port vector network analyzer to measure the scattering matrix. The magnetic excitation of the sample is achieved via inductive coupling into the top (drive) loop and the transmitted signal is picked up by the bottom (pickup) loop.

The loop antennas are 27.2 mm apart to minimize the direct magnetic coupling between them [34], which can obscure the response of the 3D metamaterial. The single spiral demonstrates a sharp fundamental resonance peak, $f_0 = \omega_0/2\pi$ at ~24.95 MHz and a dip at ~25.04 MHz at 4.3 K with a loaded quality factor of 1273. The peak and the dip in the transmission spectrum correspond to

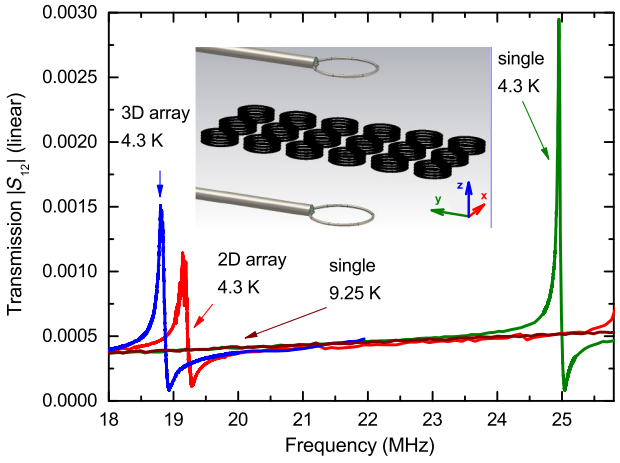

FIG. 1. Comparison of transmission $|S_{12}|$ through a single spiral (green curve), 2D array of 3×6 spirals (red curve), and 3D array of the spirals formed by stacking four substrates including 2D arrays of spirals (blue curve). The lowest resonant frequency band decreases and develops fine splitting by adding more elements to the metamaterial. The maroon curve shows the data taken at the T_c of Nb, 9.25 K, for a single spiral, where the resonant peak disappears due to enhanced ohmic losses. 2D and 3D arrays also show the same feature when the sample is heated above 9.25 K. The inset shows a schematic of the 3D metamaterial sandwiched between two rf loop antennas which are 27.2 mm apart along the z axis.

constructive and destructive interferences between the direct coupling of the loops and magnetic coupling of the loops to the metamaterial, respectively [35]. We observe higher-order modes corresponding to shorter-wavelength rf-current standing waves in the spiral, which have been extensively studied elsewhere [8,36–39]. Above the T_c of Nb, superconductivity is lost and the resonance is wiped out at 9.25 K. This demonstrates that such a compact device is not functional if made with thin films of normal metals due to the large ohmic losses. An analytical model adapted to a similar experimental configuration showed that the transmission spectrum in the absence of the spiral resonator between the loops captures the experimental transmission through the spiral taken above the T_c of the superconductor [35].

The low-temperature resonance peak shifts to a significantly smaller frequency, 19.15 MHz in the rf-transmission spectrum of the 2D array of 3×6 spirals due to a significant change in effective parameters, especially $\mu_{\mathrm{eff}}(\omega)$ [32]. The small separation distance between the spirals $\sim\lambda_0/1875$ strengthens the magnetic coupling between the individual spirals that leads to splitting of the resonant frequencies [40].

For 3D metamaterials with strong magnetic coupling in the stacking direction, the enhancement in capacitance due to interlayer interaction [41] further reduces the resonant frequency at 4.3 K down to 18.83 MHz as seen in the transmission spectrum of the 3D metamaterial. The resonant features observed in the low-temperature spectra of both 2D and 3D arrays of spirals disappear at temperatures above 9.25 K, as expected.

By considering the effective medium approximation, the frequency-dependent complex effective permeability of an array of nonmagnetic conducting SRRs is characterized with a Lorentzian function as [1]

$$\mu_{\mathrm{eff}}(\omega) = \mu'_{\mathrm{eff}}(\omega) + i\mu''_{\mathrm{eff}}(\omega) = 1 - \frac{F\omega^2}{\omega^2 - \omega_r^2 + i\Gamma\omega}, \quad (1)$$

where $\mu'_{\mathrm{eff}}(\omega)$ and $\mu''_{\mathrm{eff}}(\omega)$ are the real and imaginary parts of the effective permeability, F is the filling fraction, $\omega_r = 2\pi f_r$ is the angular center frequency of the resonance, and Γ is the damping term characterizing ohmic and radiation losses. The center frequency for the resonant bandwidth f_r is determined by the resonant parameters of individual elements f_0, as well as the mutual interactions between them [29,42].

The wavelength of the electromagnetic excitation we use is much larger than the dimensions (D_o, w, s) and separation of the spirals forming our metamaterial. Therefore, we can apply the effective medium approximation and characterize the metamaterial with $\mu_{\mathrm{eff}}(\omega)$ and $\epsilon_{\mathrm{eff}}(\omega)$. Since inductive coupling is quite prominent here, the former is the dominant effective parameter. Sharp dips of the transmission spectra just above the resonant frequencies in Fig. 1 (below the background signal set by the normal state data taken at 9.25 K) imply the presence of negative permeability. To be able to characterize the negative magnetic response of our metamaterials, we retrieve $\mu_{\mathrm{eff}}(\omega)$ from the experimental scattering matrix [41] collected by two loops connected to a network analyzer (see the inset of Fig. 1). The induced electromotive force (emf) in the pickup loop as a function of frequency due to the magnetic coupling of top loop can be written as $\mathrm{emf}(\omega)_{\mathrm{ref}} = -i\omega A\mu_0 H_z$, when there is no metamaterial between two loops and $\mathrm{emf}(\omega)_{\mathrm{meta}} = -i\omega A\mu_0\mu_{\mathrm{eff}}(\omega)H_z$, when there is metamaterial sandwiched between them. Here, A is the area of the pickup coil, μ_0 is the free space permeability, and H_z is a perpendicular component of the magnetic field. By combining these two equations, one can approximate the complex effective permeability as a ratio, $\mu_{\mathrm{eff}}(\omega) = \mathrm{emf}(\omega)_{\mathrm{meta}}/\mathrm{emf}(\omega)_{\mathrm{ref}} \sim S_{21}(\omega)_{\mathrm{meta}}/S_{21}(\omega)_{\mathrm{ref}}$. Here, it is assumed that H_z is the same in both measurements [41].

Figure 2 shows the real $\mu'_{\mathrm{eff}}(\omega)$ (red curves) and imaginary $\mu''_{\mathrm{eff}}(\omega)$ (blue curves) parts of the retrieved permeability for (a) the single spiral and (b) the 3D metamaterial composed of similar spirals. The overlapping

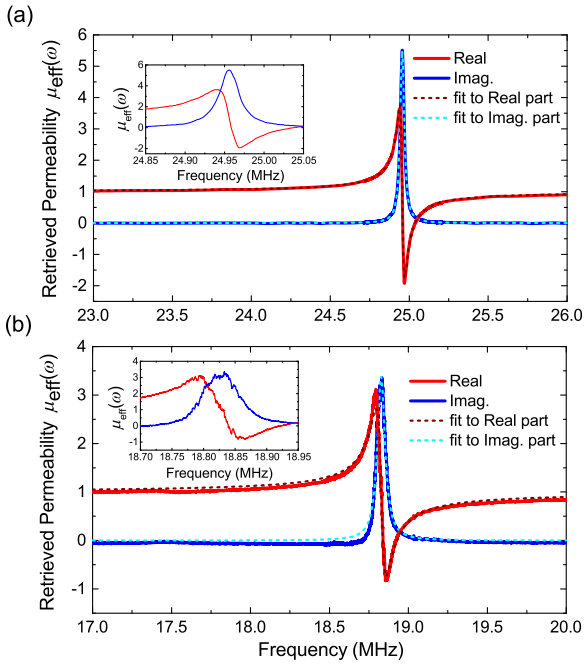

FIG. 2. Real $\mu'_{\mathrm{eff}}(\omega)$ and imaginary $\mu''_{\mathrm{eff}}(\omega)$ parts of the effective complex permeability retrieved from the experimental scattering matrix at 4.3 K for (a) a single spiral and (b) a 3D array of such spirals. The dashed maroon and cyan curves are Lorentzian fits to the retrieved data according to Eq. (1), demonstrating a significant agreement. The insets are shorter frequency-range plots of the data showing the details in the vicinity of the resonant frequency. A single smooth resonance peak of the individual spiral splits into multiple resonances for the 3D metamaterial.

dashed curves are the Lorentzian fits according to Eq. (1), which reasonably capture the retrieved data at 4.3 K. The fit parameters are $\omega_0/2\pi = 24.955$ MHz, $\Gamma/2\pi = 0.03$ MHz, and $F = 0.0068$ for the single spiral and $\omega_r/2\pi = 18.828$ MHz, $\Gamma/2\pi = 0.064$ MHz, and $F = 0.012$ for the 3D array. The enhanced loss in the 3D array compared to an individual spiral can be explained in part by the stronger inductive coupling to the excitation loops [43] and the excitation of magneto-inductive waves in the metamaterial [44]. We observe that the smooth well-defined resonance of the single spiral splits into multiple resonances with magnetic coupling into other spirals in the 3D array (see the insets of Fig. 2, showing the resonant features in detail). Just above the resonant frequency, the $\mu'_{\rm eff}(\omega)$ becomes negative in a narrow frequency band. These forbidden bands of frequencies range from 24.958 to 25.038 MHz for the single spiral and from 18.838 to 18.924 MHz for the 3D metamaterial at 4.3 K.

Having discussed the low-temperature magnetic response of the metamaterial, we now turn to the tunability of $\mu_{\rm eff}(\omega)$ as the metamaterial is heated up to a temperature above the T_c of Nb. Figures 3(a) and 3(b) show the temperature dependence of the real and imaginary parts of the retrieved $\mu_{\rm eff}(\omega)$ for the 3D metamaterial. The narrow frequency band, where the $\mu'_{\rm eff}(\omega)$ is negative, shifts to lower values as the temperature increases, as seen in Fig. 3(a). The same effect is also seen in the peaks of the $\mu''_{\rm eff}(\omega)$ that are often associated with the resonant frequencies [14,45] [see Fig. 3(b)]. The frequency shift in the spectra is a result of a decrease in the density of superconducting electrons (superfluid density) with temperature $n_s(T)$, which is inversely proportional to the square of magnetic penetration depth $\lambda_L(T)$. As the fields of the electromagnetic waves penetrate deeper into the metamaterial with increasing temperature, the total inductance of the individual spirals increases due to the enhanced kinetic inductance, $L_k \propto \lambda_L(T)\coth[t/\lambda_L(T)]$, where t is the thickness of the Nb film used to make the metamaterial [46]. The enhanced total inductance leads to a reduction in the resonant frequency [47]. Moreover, transmission decreases in magnitude and is smeared as T_c is approached due to the increasing ohmic losses arising from normal carriers, characterized by Γ in Eq. (1).

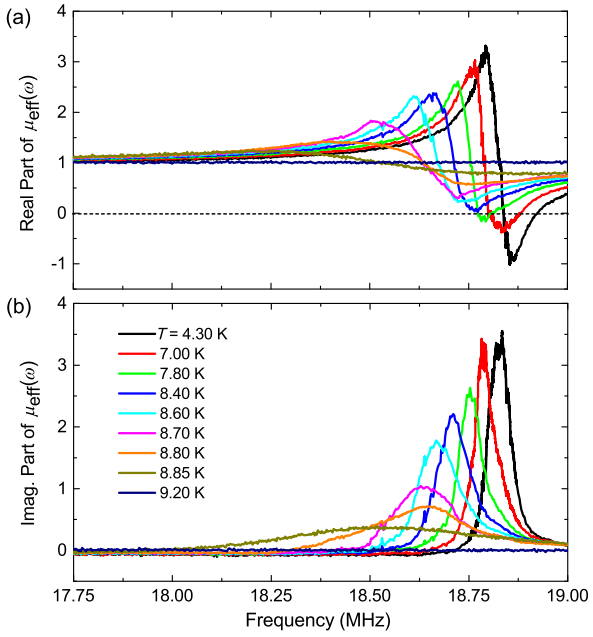

FIG. 3. Temperature evolution of (a) real $\mu'_{\rm eff}(\omega)$ and (b) imaginary $\mu''_{\rm eff}(\omega)$ parts of the retrieved permeability for the 3D metamaterial. Both the frequency band where the $\mu'_{\rm eff}(\omega)$ is negative and f_r shift to smaller values of frequency with increasing temperature due to the enhanced inductance and losses.

The narrow frequency band in the real part of $\mu_{\rm eff}(\omega)$ possesses negative values up to ~8.3 K, beyond which it starts to show near-zero and then positive values. This crossover temperature corresponds to a similar value at which we start to see a discernible downward trend in the temperature evolution of $f_r(T)$ and an upturn in the damping term $\Gamma(T)$. To study this behavior, we extract ω_r (thus f_r) and Γ as a function of temperature through fitting the retrieved $\mu_{\rm eff}(\omega)$ of the 3D metamaterial according to Eq. (1). As seen in the main panel of Fig. 4, for a long range of temperatures below T_c, both f_r and Γ are quite constant since there is no significant change in $n_s(T)$ [48]. As temperature increases, $n_s(T)$ starts to decrease, leading to a weaker response in opposing the external magnetic field. Beyond 8.3 K, we see a slight decrease (increase) in f_r (Γ) until the temperature is very near T_c. In the vicinity of T_c, we observe a steep drop (increase) in f_r (Γ) mimicking the behavior of $n_s(T)$ [$n_N(T)$, normal fluid density] in this temperature regime. Here, $\lambda_L(T)$ and

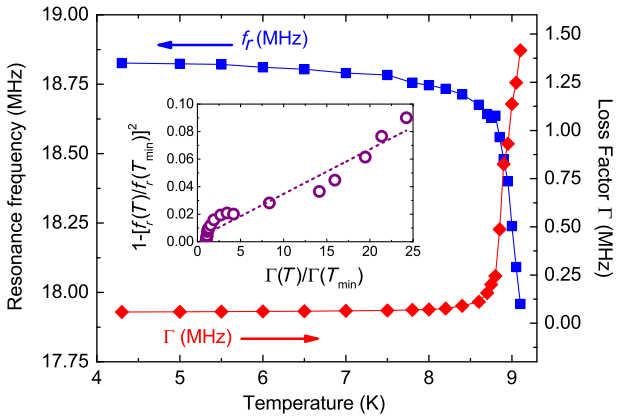

FIG. 4. Temperature evolution of the extracted resonance frequency f_r (blue squares) and damping factor Γ (red diamonds) by fitting the retrieved permeability of the 3D metamaterial according to Eq. (1). In the vicinity of T_c, f_r shows a steep drop as Γ dramatically increases. The inset is a plot showing the quantities expected to be proportional to the normal fluid density $n_N(T)$.

thus the total inductance dramatically increases (i.e., L_k diverges) and accordingly $n_s(T)$ approaches zero. At T_c, ohmic losses are enhanced due to the dominance of $n_N(T)$ over $n_s(T)$ and resonant characteristics are completely wiped out. To demonstrate this more clearly and to test the validity of our extraction, we show $1-[f_r(T)/f_r(T_{\min})]^2$ vs $\Gamma(T)/\Gamma(T_{\min})$ in the inset of Fig. 4, where $T_{\min}$ is the base temperature. Both quantities are roughly proportional to the normal fluid density $n_N(T)$, so the plot should be approximately a straight line. Though we see a nonlinearity in the vicinity of the base temperature (due to the near absence of a frequency shift), the trend is quite linear at the higher temperatures, as expected.

IV. SUMMARY

We develop a low-loss and ultrasubwavelength 3D superconducting metamaterial. The engineered compact metamaterial shows a strong magnetic response to electromagnetic waves. The resonant frequency and frequency band with negative response are precisely tuned by means of temperature without lumped elements. We observe a crossover from negative to positive $\mu'_{\text{eff}}(\omega)$ at a temperature near T_c at which a dramatic increase occurs in losses (Γ) signaling a significant decrease in superfluid density $n_s(T)$. This work contributes to ongoing research on tunable negative permeability and near-zero permeability metamaterials, which can play an important role to improve the performance and directivity of ultrasmall rf antennas.

ACKNOWLEDGMENTS

This work was supported by the U.S. Office of Naval Research through Grant No. N000140811058, the NSF-GOALI Program through Grants No. ECCS-1158644, No. NSF-DMR 1410712, and the Center for Nanophysics and Advanced Materials at the University of Maryland. For the device fabrication, we acknowledge use of facilities of the Maryland Nanocenter at the University of Maryland. The authors would like to thank Brian Straughn and John Abrahams for their technical assistance. We appreciate the helpful discussions with A. D. K. Finck, N. Maleeva, and A. Yamilov.

[1] J. B. Pendry, A. J. Holden, D. J. Robbins, and W. J. Stewart, Magnetism from conductors and enhanced nonlinear phenomena, IEEE Trans. Microwave Theory Tech. **47**, 2075 (1999).

[2] D. R. Smith, Willie J. Padilla, D. C. Vier, S. C. Nemat-Nasser, and S. Schultz, Composite Medium with Simultaneously Negative Permeability and Permittivity, Phys. Rev. Lett. **84**, 4184 (2000).

[3] Mário Silveirinha and Nader Engheta, Design of matched zero-index metamaterials using nonmagnetic inclusions in epsilon-near-zero media, Phys. Rev. B **75**, 075119 (2007).

[4] Richard Ziolkowski, Propagation in and scattering from a matched metamaterial having a zero index of refraction, Phys. Rev. E **70**, 046608 (2004).

[5] R. A. Shelby, D. R. Smith, S. C. Nemat-Nasser, and S. Schultz, Microwave transmission through a two-dimensional, isotropic, left-handed metamaterial, Appl. Phys. Lett. **78**, 489 (2001).

[6] Sajid Hussain, Jeong Min Woo, and Jae-Hyung Jang, Dual-band terahertz metamaterials based on nested split ring resonators, Appl. Phys. Lett. **101**, 091103 (2012).

[7] T. J. Yen, W. J. Padilla, N. Fang, D. C. Vier, D. R. Smith, J. B. Pendry, D. N. Basov, and X. Zhang, Terahertz magnetic response from artificial materials, Science **303**, 1494 (2004).

[8] Cihan Kurter, John Abrahams, and Steven M. Anlage, Miniaturized superconducting metamaterials for radio frequencies, Appl. Phys. Lett. **96**, 253504 (2010).

[9] Steven M. Anlage, The physics and applications of superconducting metamaterials, J. Opt. **13**, 024001 (2011).

[10] Philipp Jung, Alexey V. Ustinov, and Steven M. Anlage, Progress in superconducting metamaterials, Supercond. Sci. Technol. **27**, 073001 (2014).

[11] M. C. Ricci, Hua Xu, R. Prozorov, A. P. Zhuravel, A. V. Ustinov, and S. M. Anlage, Tunability of superconducting metamaterials, IEEE Trans. Appl. Supercond. **17**, 918 (2007).

[12] Cihan Kurter, Philippe Tassin, Alexander P. Zhuravel, Lei Zhang, Thomas Koschny, Alexey V. Ustinov, Costas M. Soukoulis, and Steven M. Anlage, Switching nonlinearity in a superconductor-enhanced metamaterial, Appl. Phys. Lett. **100**, 121906 (2012).

[13] M. Trepanier, Daimeng Zhang, Oleg Mukhanov, and Steven M. Anlage, Realization and Modeling of Metamaterials Made of rf Superconducting Quantum-Interference Devices, Phys. Rev. X **3**, 041029 (2013).

[14] C. Kurter, J. Abrahams, G. Shvets, and Steven M. Anlage, Plasmonic scaling of superconducting metamaterials, Phys. Rev. B **88**, 180510 (2013).

[15] M. C. K. Wiltshire, J. B. Pendry, I. R. Young, D. J. Larkman, D. J. Gilderdale, and J. V. Hajnal, Microstructured magnetic materials for rf flux guides in magnetic resonance imaging, Science **291**, 849 (2001).

[16] Manuel J. Freire, Ricardo Marques, and Lukas Jelinek, Experimental demonstration of a $\mu=-1$ metamaterial lens for magnetic resonance imaging, Appl. Phys. Lett. **93**, 231108 (2008).

[17] Manuel J. Freire, Lukas Jelinek, Ricardo Marques, and Mikhail Lapine, On the applications of $\mu=-1$ metamaterial lenses for magnetic resonance imaging, J. Magn. Reson. **203**, 81 (2010).

[18] M. J. Freire and R. Marques, Planar magnetoinductive lens for three-dimensional subwavelength imaging, Appl. Phys. Lett. **86**, 182505 (2005).

[19] A. Kurs, A. Karalis, R. Moffatt, J. D. Joannopoulos, P. Fisher, and M. Soljacic, Wireless power transfer via strongly coupled magnetic resonances, Science **317**, 83 (2007).

[20] Guy Lipworth, Joshua Ensworth, Kushal Seetharam, Da Huang, Jae Seung Lee, Paul Schmalenberg, Tsuyoshi Nomura, Matthew S. Reynolds, David R. Smith, and Yaroslav Urzhumov, Magnetic metamaterial superlens for increased range wireless power transfer, Sci. Rep. **4**, 3642 (2014).

[21] R. J. Sedwick, Long range inductive power transfer with superconducting oscillators, Ann. Phys. (N.Y.) **325**, 287 (2010).
[22] Bingnan Wang, Koon Hoo Teo, Tamotsu Nishino, William Yerazunis, John Barnwell, and Jinyun Zhang, Experiments on wireless power transfer with metamaterials, Appl. Phys. Lett. **98**, 254101 (2011).
[23] F. Bilotti, A. Alu, and L. Vegni, Design of miniaturized metamaterial patch antennas with μ-negative loading, IEEE Trans. Antennas Propag. **56**, 1640 (2008).
[24] J. P. Turpin, J. A. Bossard, K. L. Morgan, D. H. Werner, and P. L. Werner, Reconfigurable and tunable metamaterials: A review of the theory and applications, Int. J. Antennas Propag. **2014**, 429837 (2014).
[25] R. W. Ziolkowski and A. Kipple, Application of double negative materials to increase the power radiated by electrically small antennas, IEEE Trans. Antennas Propag. **51**, 2626 (2003).
[26] R. W. Ziolkowski and A. Erentok, Metamaterial-based efficient electrically small antennas, IEEE Trans. Antennas Propag. **54**, 2113 (2006).
[27] R. C. Hansen, *Electrically Small, Superdirective, and Superconducting Antennas* (A.J. Wiley and Sons, Hoboken, 2006).
[28] Juan D. Baena, Ricardo Marqués, Francisco Medina, and Jesús Martel, Artificial magnetic metamaterial design by using spiral resonators, Phys. Rev. B **69**, 014402 (2004).
[29] M. Gorkunov, M. Lapine, E. Shamonina, and K. H. Ringhofer, Effective magnetic properties of a composite material with circular conductive elements, Eur. Phys. J. B **28**, 263 (2002).
[30] S. Massaoudi and I. Huynen, Multiple resonances in arrays of spiral resonators designed for magnetic resonance imaging, Microwave Opt. Technol. Lett. **50**, 1945 (2008).
[31] Ilya V. Shadrivov, David A. Powell, Steven K. Morrison, Yuri S. Kivshar, and Gregory N. Milford, Scattering of electromagnetic waves in metamaterial superlattices, Appl. Phys. Lett. **90**, 201919 (2007).
[32] Philippe Gay-Balmaz and Olivier J. F. Martin, Electromagnetic resonances in individual and coupled split-ring resonators, J. Appl. Phys. **92**, 2929 (2002).
[33] David Powell, Mikhail Lapine, Maxim Gorkunov, Ilya Shadrivov, and Yuri Kivshar, Metamaterial tuning by manipulation of near-field interaction, Phys. Rev. B **82**, 155128 (2010).
[34] C. Kurter, A. P. Zhuravel, J. Abrahams, C. L. Bennett, A. V. Ustinov, and S. M. Anlage, Superconducting rf metamaterials made with magnetically active planar spirals, IEEE Trans. Appl. Supercond. **21**, 709 (2011).
[35] B. G. Ghamsari, J. Abrahams, S. Remillard, and S. M. Anlage, High-temperature superconducting spiral resonator for metamaterial applications, IEEE Trans. Appl. Supercond. **23**, 1500304 (2013).
[36] Alexander P. Zhuravel, Cihan Kurter, Alexey V. Ustinov, and Steven M. Anlage, Unconventional rf photoresponse from a superconducting spiral resonator, Phys. Rev. B **85**, 134535 (2012).
[37] Behnood G. Ghamsari, John Abrahams, Stephen Remillard, and Steven M. Anlage, High-temperature superconducting multi-band radio-frequency metamaterial atoms, Appl. Phys. Lett. **102**, 013503 (2013).
[38] Vijaykumar Ramaswamy, Jerris W. Hooker, Richard S. Withers, Robert E. Nast, William W. Brey, and Arthur S. Edison, Development of a 14C-Optimized 1.5-mm high temperature superconducting NMR probe, J. Magn. Reson. **235**, 58 (2013).
[39] N. Maleeva, M. V. Fistul, A. Karpov, A. P. Zhuravel, A. Averkin, P. Jung, and A. V. Ustinov, Electrodynamics of a ring-shaped spiral resonator, J. Appl. Phys. **115**, 064910 (2014).
[40] Michael C. Ricci and Steven M. Anlage, Single superconducting split-ring resonator electrodynamics, Appl. Phys. Lett. **88**, 264102 (2006).
[41] W.-C. Chen, C. M. Bingham, K. M. Mak, N. W. Caira, and W. J. Padilla, Extremely subwavelength planar magnetic metamaterials, Phys. Rev. B **85**, 201104 (2012).
[42] Mikhail Lapine, David Powell, Maxim Gorkunov, Ilya Shadrivov, Ricardo Marques, and Yuri Kivshar, Structural tunability in metamaterials, Appl. Phys. Lett. **95**, 084105 (2009).
[43] R. R. A. Syms, I. R. Young, and L. Solymar, Low-loss magneto-inductive waveguides, J. Phys. D **39**, 3945 (2006).
[44] G. P. Tsironis, N. Lazarides, and I. Margaris, Wide-band tuneability, nonlinear transmission, and dynamic multistability in SQUID metamaterials, Appl. Phys. A **117**, 579 (2014).
[45] Hou-Tong Chen, Hao Yang, Ranjan Singh, John F. O'Hara, Abul K. Azad, Stuart A. Trugman, Q. X. Jia, and Antoinette J. Taylor, Tuning the Resonance in High-Temperature Superconducting Terahertz Metamaterials, Phys. Rev. Lett. **105**, 247402 (2010).
[46] B. W. Langley, S. M. Anlage, R. F. W. Pease, and M. R. Beasley, Magnetic penetration depth measurements of superconducting thin films by a microstrip resonator technique, Rev. Sci. Instrum. **62**, 1801 (1991).
[47] S. M. Anlage, H. J. Snortland, and M. R. Beasley, A current controlled variable delay superconducting transmission line, IEEE Trans. Magn. **25**, 1388 (1989).
[48] M. S. Pambianchi, S. M. Anlage, E. S. Hellman, E. H. Hartford, M. Bruns, and S. Y. Lee, Penetration depth, microwave surface resistance, and gap ratio in NbN and $Ba_{1-x}K_xBiO_3$ thin films, Appl. Phys. Lett. **64**, 244 (1994).